

# 2D Layered Perovskites

## Solution Processable Materials

The recent discovery that single-layer 2D perovskites can be prepared using solution processing techniques<sup>1</sup> has been followed by enormous research into optoelectronic applications of 2D perovskites including light emitting diodes (LEDs),<sup>2</sup> phototransistors,<sup>3</sup> and solar cells.<sup>4</sup>

## Tunable Emission Wavelength

Photoluminescent 2D perovskites have an emission wavelength that changes depending on the layer thickness and the choice of amine and halide. We offer an excellent portfolio of the most popular 2D perovskite compositions for photoluminescence based devices.

## Improved Moisture Stability

Solar cells fabricated with 2D perovskites have improved stability in moist air compared to 3D perovskites.<sup>4</sup>



Formula	Cat. No.	Layer Thickness	$(\text{RNH}_3)_2(\text{MeNH}_3)_{n-1}\text{Pb}_n\text{X}_{3n+1}$		
			R	X	n
$(\text{BA})_2\text{PbI}_4$	910961	n=1	Bu	I	1
$(\text{BA})_2\text{PbBr}_4$	910953	n=1	Bu	Br	1
$(\text{PEA})_2\text{PbI}_4$	910937	n=1	PE	I	1
$(\text{PEA})_2\text{PbBr}_4$	910945	n=1	PE	Br	1
$(\text{BA})_2(\text{MA})\text{Pb}_2\text{I}_7$	912816	n=2	Bu	I	2
$(\text{BA})_2(\text{MA})_2\text{Pb}_3\text{I}_{10}$	912557	n=3	Bu	I	3
$(\text{BA})_2(\text{MA})_3\text{Pb}_4\text{I}_{13}$	914363	n=4	Bu	I	4
$(\text{BA})_2(\text{MA})_4\text{Pb}_5\text{I}_{16}$	912301	n=5	Bu	I	5

BA = n-butylammonium; PEA = 2-phenylethylammonium; MA = methylammonium, Bu=n-butyl, PE=2-phenylethyl

## References:

- 1) Dou, L.; Wong, A. B.; Yu, Y.; Lai, M.; Kornienko, N.; Eaton, S. W.; Fu, A.; Bischak, C. G.; Ma, J.; Ding, T.; Ginsberg, N. S.; Wang, L.-W.; Alivisatos, A. P.; Yang, P. *Science* **2015**, *349*, 1518. DOI: 10.1126/science.aac7660
- 2) Yuan, M.; Quan, L. N.; Comin, R.; Walters, G.; Sabatini, R.; Voznyy, O.; Hoogland, S.; Zhao, Y.; Beauregard, E. M.; Kanjanaboos, P.; Lu, Z.; Kim, D. H.; Sargent, E. H. *Nat. Nanotechnol.* **2016**, *11*, 872. DOI: 10.1038/NNANO.2016.110
- 3) Shao, Y.; Liu, Y.; Chen, X.; Chen, C.; Sarpkaya, I.; Chen, Z.; Fang, Y.; Kong, J.; Watanabe, K.; Taniguchi, T.; Taylor, A.; Huang, J.; Xia, F. *Nano Lett.* **2017**, *17*, 7330. DOI: 10.1021/acs.nanolett.7b02980
- 4) Cao, D. H.; Stoumpos, C. C.; Farha, O. K.; Hupp, J. T.; Kanatzidis, M. G. *J. Am. Chem. Soc.* **2015**, *137*, 7843. DOI: 10.1021/jacs.5b03796

[SigmaAldrich.com/perovskite](http://SigmaAldrich.com/perovskite)

MilliporeSigma is the U.S. and Canada Life Science business of Merck KGaA, Darmstadt, Germany.

© 2022 Merck KGaA, Darmstadt, Germany and/or its affiliates. All Rights Reserved. MilliporeSigma, the vibrant M, and Sigma-Aldrich are trademarks of Merck KGaA, Darmstadt, Germany or its affiliates. All other trademarks are the property of their respective owners. Detailed information on trademarks is available via publicly accessible resources.

MS\_AD9822EN 43729 09/2022

MilliporeSigma is the U.S. and Canada Life Science business of Merck KGaA, Darmstadt, Germany.

**Sigma-Aldrich®**  
Lab & Production Materials

# Sustainable Long-Term and Wide-Area Environment Monitoring Network Based on Distributed Self-Powered Wireless Sensing Nodes

Di Liu, Chengyu Li, Pengfei Chen, Xin Zhao, Wei Tang,\* and Zhong Lin Wang\*

Environmental monitoring of local climatic variations plays a vital role in the research on global warming, species diversity, ecological sustainability, and so on. Traditional monitoring technologies, such as meteorological stations or satellite imagery, can give an overall environment picture but at high cost, high energy consumption, and with insufficient regional details. Here, a networking system made of low-cost, maintenance-free, and distributed self-powered wireless monitoring nodes is proposed, aimed at establishing a sensing system for long-term and wide-area environment monitoring. It is demonstrated that, as driven by gentle wind, these distributed nodes are able to monitor temperature, humidity, and atmospheric pressure automatically, and then transfer the sensing data to receiving terminals wirelessly using triboelectric nanogenerators as energy harvesting technologies. The longest transmitting distance is 2.1 km. Additionally, a sensing network is formed. By utilizing several nodes, a 2-km<sup>2</sup> region is covered, and the information can be transmitted live using a relay-technology. Furthermore, the node is demonstrated to work for weeks, and continuously send back environmental data. Since the nodes are portable and the embedded sensors are customizable, it is anticipated that the system can be multifunctional and applied in many natural areas, such as forests, prairies, mountains, lake regions, and so on.

## 1. Introduction

Climate change has attracted wide attention in recent years due to its significant influence on biodiversity,<sup>[1,2]</sup> agriculture,<sup>[3]</sup> ecology,<sup>[4,5]</sup> health burden,<sup>[6]</sup> and so on,<sup>[7,8]</sup> which are vital for society sustainable development.<sup>[9]</sup> Its local monitoring is useful to our daily life, e.g., weather prediction,<sup>[10]</sup> wildfire prevention,<sup>[11]</sup> rare species protection,<sup>[12]</sup> etc. However, the common method for environment monitoring is satellite imaging<sup>[13]</sup> or meteorological station, which gives an overall environment information but at high cost, enormous energy consumption, and insufficient regional details.

Recent studies tend to address this problem by using distributed monitoring nodes.<sup>[14]</sup> However, sustainable power supply is required. Cabling makes the monitoring expensive and difficult to relocate once they are installed.<sup>[15]</sup> Batteries will improve the movability but require maintenance once they run out of power.<sup>[16]</sup> Solar panels could harness the ambient sun energy, but a requirement of sunlight make it limited due to the shaded

or hidden working area as well as long-evening and poor weather condition.<sup>[17,18]</sup> The latter could be solved by a built-in rechargeable battery, which, however, hinders the whole system's long-time usage (e.g., for years), owing to the battery's limited lifetime. Considering the abundant mechanical energy in ambient, wind-driven prototypes on the basis of electromagnetic principle are proposed.<sup>[19–21]</sup> However, due to the nature of electromagnetic conversion, it takes low energy conversion under low frequency at low wind speed. Recently, triboelectric nanogenerators (TENG) are developed for its high-energy-conversion under low-frequency impacts.<sup>[22]</sup> Researchers demonstrate some prototypes by using TENG to collect the ambient mechanical energy and then power the environmental sensors or systems,<sup>[23–27]</sup> e.g., humidity,<sup>[28,29]</sup> temperature,<sup>[30]</sup> greenhouse gas (CO<sub>2</sub>),<sup>[31]</sup> and toxic gas (CO, NO<sub>2</sub>).<sup>[32,33]</sup> Additionally, Zhang demonstrated a self-powered wireless buoy system, driven by water wave TENG, which can sense acceleration, magnetic intensity, and temperature data with a transmitting range of 15 m.<sup>[34]</sup> Xu<sup>[35]</sup> and Chen<sup>[36]</sup> demonstrated self-powered instantaneous wireless humidity sensing system

D. Liu, C. Li, P. Chen, X. Zhao, W. Tang, Z. L. Wang  
CAS Center for Excellence in Nanoscience  
Beijing Institute of Nanoenergy and Nanosystems  
Chinese Academy of Sciences  
Beijing 100083, China  
E-mail: tangwei@binn.cas.cn; zhong.wang@mse.gatech.edu

D. Liu, C. Li, P. Chen, W. Tang, Z. L. Wang  
School of Nanoscience and Technology  
University of Chinese Academy of Sciences  
Beijing 100049, China

W. Tang  
Institute of Applied Nanotechnology  
Jiaxing, Zhejiang 314031, P. R. China

Z. L. Wang  
School of Materials Science and Engineering  
Georgia Institute of Technology  
Atlanta, GA 30332-0245, USA

 The ORCID identification number(s) for the author(s) of this article can be found under <https://doi.org/10.1002/aenm.202202691>.

DOI: 10.1002/aenm.202202691

with a transmitting distance 50 cm and 3 m, respectively. However, among them, the communication distance is relatively short. More importantly, a monitoring network covering a wide area is barely reported, which requires a continuous and long period of time operations in natural environment.

Here, we present a self-powered long-term and wide-area environment monitoring network, constructed from low-cost, maintenance-free and distributed TENG-driven sensing nodes. A breeze-wind-driven configuration with power management circuit is designed. Environment temperature, humidity, and atmospheric pressure can be detected and transmitted automatically to the receiver through a 433 MHz radio frequency. And a cellphone program is developed to display the sensing data in real time. Compared with the previous work, the advance of our work involves: (1) a universal design scheme is proposed for self-powered wireless environment monitoring nodes based on TENG, (2) the start-up wind speed of each sensing node is extended downward to  $1 \text{ m s}^{-1}$ , (3) long-term and wide-area monitoring approach is established, covering several square kilometers, and lasting for weeks. We anticipate that, as the present system expanded, it would be more multifunctional and significant in local environment monitoring, applicable to many natural areas, such as forest, prairie, mountains, lakes regions, and so on.

## 2. Results

Wide-area and long-term monitoring of local environment exhibits great significance on climate change analysis, which is closely related to our daily life, ecological balance, and sustainable development. **Figure 1a** shows a self-powered wireless sensing network to achieve a long-term and wide-area local temperature, humidity, and atmospheric pressure monitoring. **Figure S1a** (Supporting Information) depicts the scheme of the network, which comprises of a monitoring node that senses the environment data and then transmits the data to a receiver. And then, a cell phone program is developed to display all data in real time. The node on the network is powered by a wind-TENG (**Figure 1b**). The wind-TENG is composed of a vertical wind mill and a freestanding-mode TENG, linked by an acrylic roller. The TENG part contains printed circuit boards (PCB), three elongated fiber strips, and a fluorinated ethylene propylene (FEP) coated acrylic plate. The fabrication begins with sticking the elongated fiber strips to the PCB as stator (**Figure 1c** upper image), then mounting the stator to the top shell rigidly. Subsequently, the FEP-coated acrylic plate rotor (**Figure 1c** lower image) is fixed on the roller leaving a gap about 1 mm from the stator (**Figure S1b**, Supporting Information). Finally, the TENG part is enclosed by the acrylic shell. More detailed fabrication can be found in Experimental Section. As the wind blows, electricity is generated due to the triboelectrification between the fiber and FEP, as well as the induced charges on the surface of the stator. The relative rotation motions results in alternating flow of electrons between the two groups of induction electrodes on PCB (**Figure S1c**, Supporting Information).

Notably, previous studies usually place the rotor above the stator.<sup>[37–39]</sup> Considering the rotor possess a thin and large substrate, the problem of electrostatic adsorption between the

stator and rotor cannot be neglected. As the charge density further increases, the problem gets even worse, so that the TENG stops working anymore. In our design, this problem was addressed by simply placing the rotor below the stator, as shown in **Figure 1e**. Therefore, the gravity of the rotor competes with the electrostatic force, so that an air gap exists stably between the rotor and stator. Therefore, friction resistance dramatically decreases, and the TENG starts to work at light air (around  $1 \text{ m s}^{-1}$ ), as **Figure 1f** shows. **Table S1** (Supporting Information) are attached to exhibit the list of wind scale.

The characterization of the wind-TENG is shown in **Figure 2**. Here, an electric fan with adjustable speed is applied to mimic the wind (**Figure S2**, Supporting Information). It can be seen from **Figure 2a**, as the wind speed increases, the device's open circuit voltage ( $V_{oc}$ ) and transferred charge quantity ( $Q_{sc}$ ) both increases. They also show a rapid growth within the wind speed below  $4 \text{ m s}^{-1}$ , then seem to saturate when the wind speed exceeds  $4 \text{ m s}^{-1}$ . The maximum peak to peak value of  $V_{oc}$  is 6 kV and the maximum  $Q_{sc}$  is around  $0.38 \mu\text{C}$ . **Figure 2b** illustrates the output power and current under various loads, with a wind speed of  $3 \text{ m s}^{-1}$ . It is found that, as the external resistance increased, the current apparently decreased. And the instantaneous output power was maximized at a load of  $400 \text{ M}\Omega$ , resulting in a peak power of 4 mW. And it is superior to other works in the literature (piezoelectric nanogenerator,<sup>[40]</sup> triboelectric nanogenerator,<sup>[41,42]</sup> electromagnetism generator<sup>[43,44]</sup>), as shown in **Figure 2c**. The detailed output performance can be found in **Figure S3** (Supporting Information). Further, the device's torque is examined and illustrated in **Figure 2d**. The torque is below 5 mN m when the rotation speed is  $45 \text{ r min}^{-1}$  (driven by a motor), which indicates that a slight wind can trigger the TENG to work.<sup>[45]</sup> As for the robustness, the  $Q_{sc}$  is tested under different humidity and temperature, respectively (**Figure 2e**, **Figure S4**, Supporting Information). It shows that the average  $Q_{sc}$  is  $0.327 \mu\text{C}$  with a standard deviation 6% when the humidity changes from 20%RH to 77%RH. And the average  $Q_{sc}$  is  $0.333 \mu\text{C}$  with a standard deviation 9% when temperature changes from  $-15$  to  $33 \text{ }^\circ\text{C}$ . Thus, the humidity and temperature have little influence on the  $Q_{sc}$ , which ensure the TENG stable working under various environment. Additionally, **Figure 2f** and **Figure S5** (Supporting Information) illustrate the durability of wind-TENG during 3 million rotation cycles. The device's half-wave voltage remains stable, achieving an average value of 2.1 kV with a variation about  $\pm 8\%$ .

In order to improve the energy storage efficiency and then supply electronic circuits with applicable voltage, a power manage unit (PMU) is designed, as shown in **Figure 3a**. The PMU consists of a power management (PMM) circuit for fast charging and a under voltage lockout (UVLO) circuit for load protection. The PMM was designed based on a silicon controlled rectifier (SCR) topology circuit by using a capacitor, a thyristor, Zener diodes and a buck circuit. The UVLO was designed based on a chip of LTC3588. The detailed circuit scheme, mechanism and components parameters can be found in **Figure S6**, **Note S1**, and **Table S2** (Supporting Information) respectively. Voltage variations on typical nodes in the power manage circuit are plotted in **Figure 3b**. At the beginning, the full-bridge circuit rectifies the alternating wave, and then the electricity was stored to capacitor  $C_1$ . Subsequently, the voltage

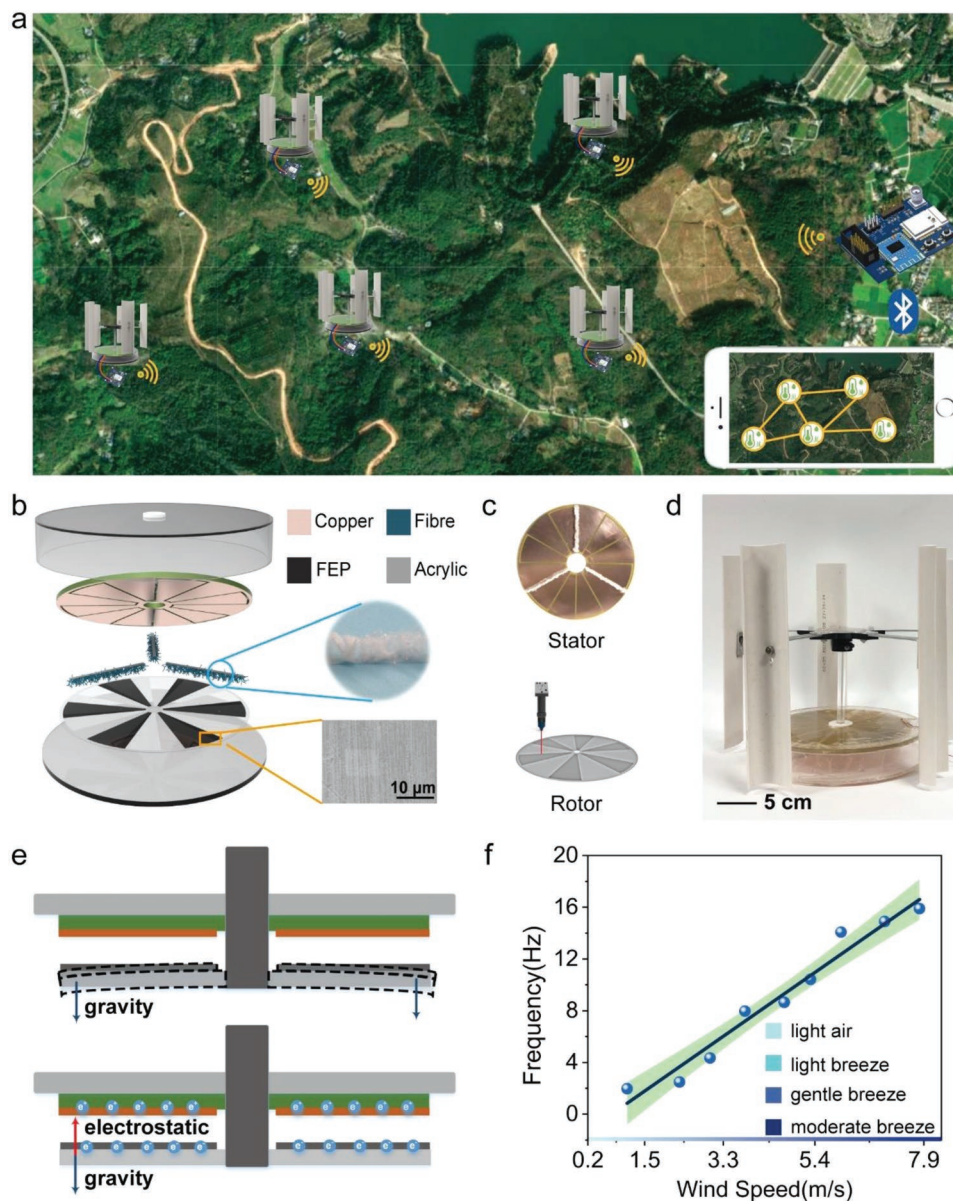


**Figure 1.** Prototype of the self-powered wireless sensing network. a) Schematic of a self-powered wireless sensing network. b) Exploded view of the TENG structure consisting of acrylic shell, pcb stator, fiber, and FEP coated rotor. c) Image of the PCB stator with fiber sticks and all-laser fabricated rotor with FEP film coated. d) Camera image of the wind-TENG including the wind mill actuator and freestanding mode TENG. e) Illustration advantage of the TENG design: the rotor border experiences a gravity force which can balance the electrostatic force to avoid the adsorption phenomenon. f) Performance of the wind-TENG operating under different kind of wind, and it starts at light air.

of  $C_1$  increases until breaking down the Zener diodes to trigger the SCR to turn on, so that the electricity in  $C_1$  can be extracted quickly to the  $C_{store}$  through the buck circuit. When the voltage of  $C_1$  return to zero, the SCR turns off and waits for the next trigger. Meanwhile, once the voltage of the  $C_{store}$  ( $V_{C_{store}}$ ) reaches to 5 V, the UVLO outputs a constant voltage ( $V_{load}$ ) of 3.3 V. And as the energy is consumed, the UVLO will cut off, when the voltage of the  $C_{store}$  is below 4 V. Therefore, the  $V_{load}$  is automatically controlled by UVLO and the energy harvested by the TENG, showing a totally self-powered functionality.

Figure 3c,d illustrates the performance of the PMM-integrated TENG. At a wind speed of  $3 \text{ m s}^{-1}$ , it is able to charge a

1 or 10 mF capacitor to 3.6 V, within 1 or 10 min, respectively. From the charging curve of the 10 mF capacitor (Figure 3d), the PMM has improved the charging speed by around 20 times, compared to the full-bridge circuit and the traditional electromagnetic transformer. Additionally, the improvement is significant, as long as the input impact frequency is higher than 1 Hz (Figure S7, Supporting Information). Subsequently, a self-powered temperature and humidity monitoring node is fabricated by connecting the wind-TENG, PMU and a commercial thermohygrometer, as shown in Figure 3e. A 3.3 mF capacitor is charged to 5 V after 280 s, and then the thermohygrometer starts its initialization and works continuously. When the wind

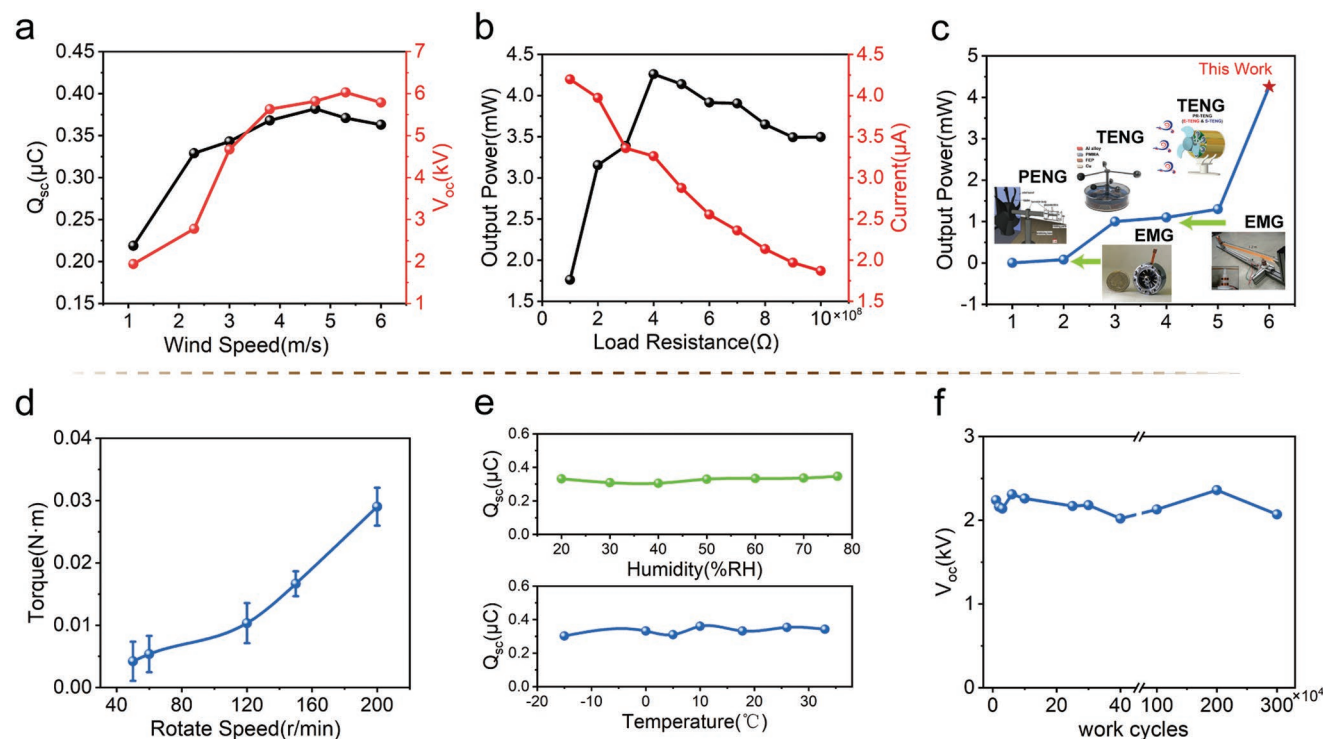


**Figure 2.** Characterization of the wind-TENGs. a) The variation of open circuit voltage (peak to peak) and transfer charge quantity as the wind speed increases. b) Illustration of the output power and under various load resistance with a wind speed  $3 \text{ m s}^{-1}$ . c) At wind speed  $3 \text{ m s}^{-1}$ , the comparison of output power between this work and other previous works, such as piezoelectric nanogenerator (PENG), triboelectric nanogenerator (TENG) and electromagnetism generator (EMG). d) Illustration of the torque variation under incremental rotate speed. e) At the wind speed  $3 \text{ m s}^{-1}$ , the variation of the transferred charge quantity while the humidity varies from 20% to 77% with a  $Q_{sc}$  standard deviation 6% and the temperature varies from  $-15$  to  $34 \text{ }^{\circ}\text{C}$  with a  $Q_{sc}$  standard deviation 9%. f) The durability test of the wind-TENG suffering 3 million rotation cycles.

stops, the thermohygrometer can still operate normally for a temporary time. Moreover, when the wind blows again, the system quickly wakes up again.

Furthermore, a series of experiments were performed in natural environment (Experimental Section and Figure S8, Supporting Information) and results are illustrated in Figure 4. Figure 4a shows the real-time curve of the TENG's transferred charges. Since the natural wind blows intermittently, the charge transferring is also intermittent. The related wind information is summarized in Figure S9 (Supporting Information). It can be found that, the wind-TENG outputs charge around  $250 \text{ nC}$  per cycle at the gentle breeze (wind speed ranging from  $3.5$  to  $5.4 \text{ m s}^{-1}$ ), which is slight lower than that tested in laboratory. But when the wind speed becomes higher, faster rotation makes the flat rotor contact better with fiber, which increases the transferred charge quantity. Notably, when the charge density gets high, it will remain stable for a long time, unless the wind stops, which can be seen from the red and blue curve in Figure 4a. Figure 4b shows a typical charging curve of a  $10 \text{ mF}$  capacitor with PMM. It takes around  $25 \text{ min}$  to be charged to  $3.6 \text{ V}$ , when the gentle and moderate breeze ( $6.5 \text{ m s}^{-1}$  of instantaneous wind speed) both exist. And during this period, the charging speed of the capacitor varies at intervals, due to the time-varying natural wind blowing. Figure 4c demonstrates a self-powered thermohygrometer. Here, a  $3.3 \text{ mF}$  capacitor is charged for around  $360 \text{ s}$ , and then the thermohygrometer starts to work. Afterward, it keeps working continuously under a gentle breeze.

Subsequently, we designed ten wireless sensing nodes, capable of sensing temperature, humidity and atmospheric pressure, and the corresponding receiver terminal, as well as the display program (Figures S10 and S11, Supporting Information). Each sensing node was fabricated by integrating TENG, PMU, sensors and transmitters (Figure S11c, Supporting Information). Afterward, all nodes were placed in various locations around the receiver, as shown in Figure 5a. Nodes 1, 2, 3, 5, and 7 are picked up to analyze our distributed network. The other nodes' sensing results can be found in Figure S12 (Supporting Information). The distance away from the receiver for the nodes 1, 2, 3, 5, and 7 are respectively  $120 \text{ m}$ ,  $780 \text{ m}$ ,  $2.1 \text{ km}$ ,  $1.1 \text{ km}$ , and  $100 \text{ m}$ . Figure 5b plots the voltage variation of the  $C_{store}$  in node 3 and node 5. Under a moderate breeze, node 5 takes  $8 \text{ min}$  to complete the initial sensing and data transmitting. Whereas, under a gentle breeze, the node 3 spends about  $80 \text{ min}$  to complete the initial sensing and data transmitting. The red curve shows the UVLO's power supply for terminal corresponding to the blue curve. It is worth noting that, after the initial sensing, the following sensing process takes less time, owing to the remaining energy stored in the capacitor. Figure 5c shows the data acquired from nodes 1, 2, 7, lasting for  $12 \text{ h}$ . Detailed monitoring can be found in Figure S13 and Movie S1 (Supporting Information). It is interesting to find that the atmospheric pressure in Node 2 is a bit higher than that in the other two, for Node 2 is placed in a wide open area (Experimental Section) with higher temperature and lower humidity.<sup>[46]</sup> Moreover, there

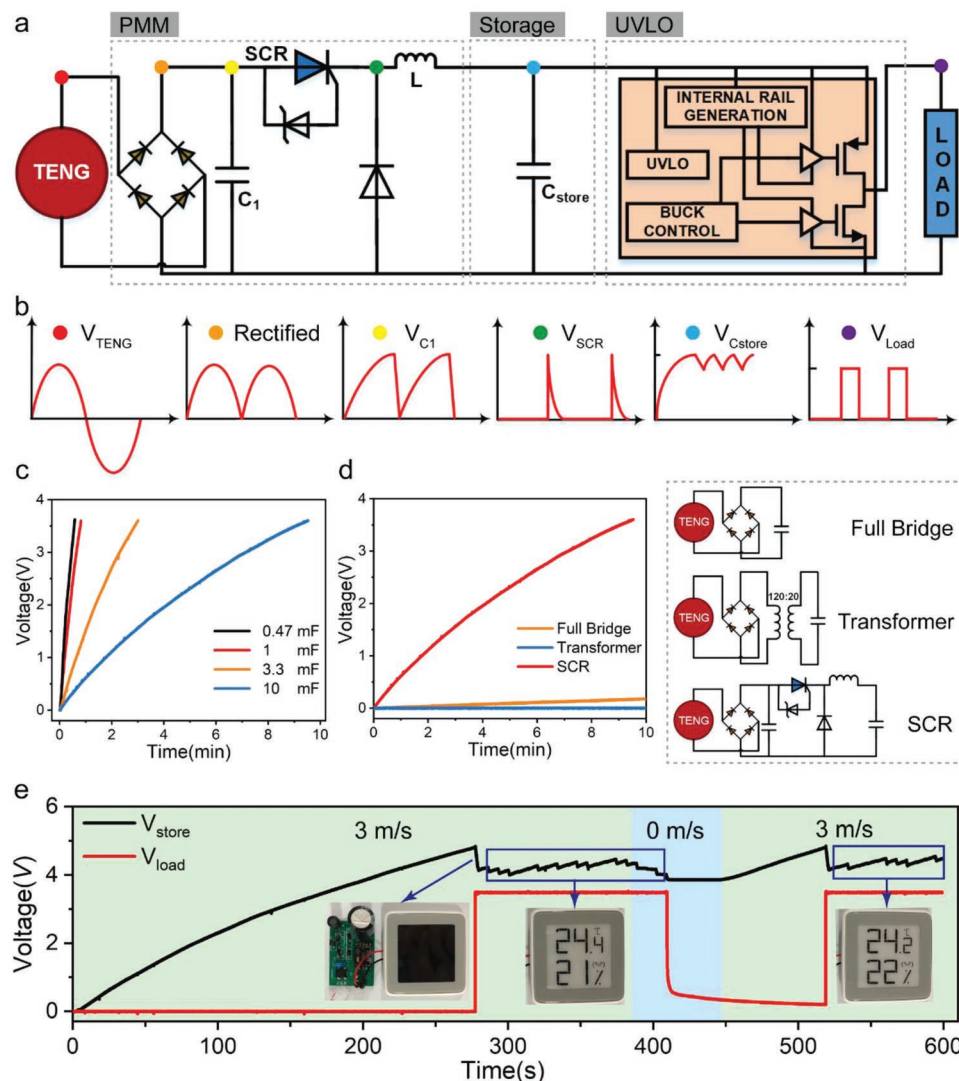


**Figure 3.** Schematic design and performance of PMU. a) Schematic design of the PMU. b) Illustration the voltage variation on typical nodes of PMU. c) Output performance of the PMM-integrated TENG. d) Performance comparison of the SCR power management circuit, full-bridge circuit and transformer circuit by charging a 10 mF capacitor. The three kinds of topological circuits are shown in right block. e) The working process of a self-powered temperature and humidity monitoring node.

is abundant wind energy around locations of Nodes 1 and 7, for more sensing data are obtained. Additionally, since the Node 1 and Node 7 are close, they show similar atmospheric pressure. And compared to Node 7, Node 1 shows a higher humidity, for it is close to the lush grass and damp soil.

Furthermore, we demonstrate a long-term environment monitoring by node 7 for more than half a month, proving the robustness of the self-powered sensing node. The purple, blue and green curves represent the local variation of atmospheric pressure, temperature and humidity, respectively. And the data are recorded from April 13th to April 30th, in Huairou District, of Beijing, in China. From the temperature curve, we can see that, the daily highest temperature reasonably arose around midday, and that value kept going up for the first 10 days, due to that spring was coming. After that, there came a rainy day (April 28th), and the daily highest temperature apparently decreased.

Moreover, during our monitoring, there happened a dust storm for several days, as shown in the yellow area in **Figure 6**. The storm came up with a strong wind, which began at around 12 o'clock on April 20th. The high-dense data suggests the storm lasting for almost two days (April 20th and 21th). On the contrary, the weather forecast the dust storm for one day, only on April 21th (Figure S14a, Supporting Information), which suggests the accuracy of the local monitoring. And it is also implied the advantage of our monitoring nodes' stability for working in the sandstorm, compared to the solar-panel-supplied monitoring systems. Furthermore, it is interesting to find that, before the rainy day (Figure 6a), the local temperature went down and the humidity increased to a very high level. And after the rain, the atmospheric got higher and the humidity decreased as well (Figure 6c). Notably, the reason that no data were received at the rainy day should be the calm wind (Figure S14c, Supporting Information), as well as the suppressed TENG

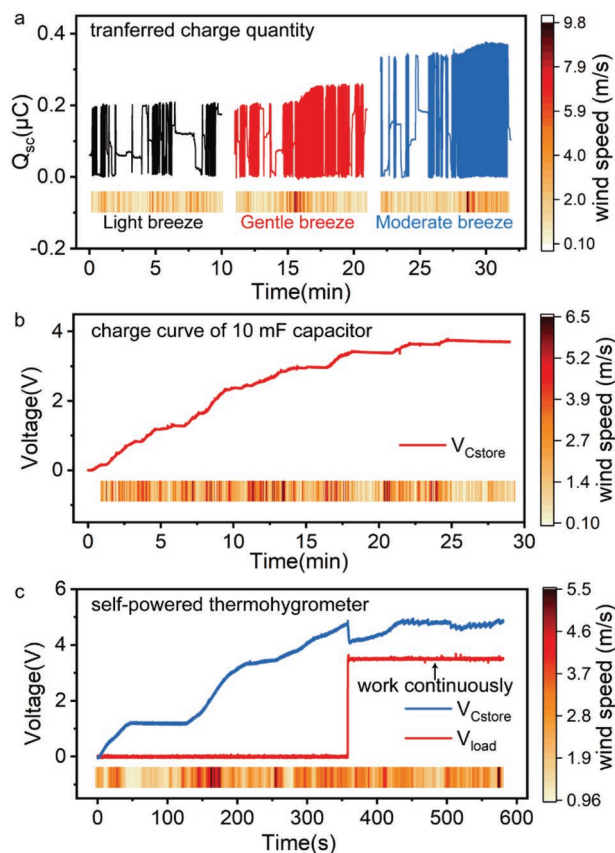


**Figure 4.** The experiments of wind-TEG, PMU and self-powered thermohygrometer tested in natural environment. a) The real-time curve of TENG's transferred charges. The heat map demonstrates the corresponding wind speed measured in real time. b) A typical charging curve of a 10 mF capacitor charged with PMM under natural wind. c) The working process of a self-powered thermohygrometer.

output caused by the wetting fiber inside the device. However, after the rainy day, when the fiber became dry and the wind blew, the node woke up to monitor the environment again, as shown in Figure 6c. This minor defect can be easily solved by waterproof measures demonstrated in Figure S15 (Supporting Information).

### 3. Discussion

Distributed, long-term and wide-area environment monitoring for analyzing climate change, exhibits great significance on our daily life, ecological balance and sustainable development. Traditional technologies, such as meteorological station or satellite imagery, can give an overall environment monitoring but at high cost, high energy consumption, and insufficient regional details. For example, as Figure S14a (Supporting Information) shows, the weather station forecast that the storm would occur on April 21 and lasting for 1 day. But in fact, the storm happened early, and lasted for around 2 days, around our monitoring locations.

In summary, we demonstrated a sustainable long-term and wide-area environment monitoring network, based on low-cost,

maintenance-free, and distributed TENG-driven sensing nodes. The network achieves real-time, distributed and wireless environment monitoring. Specifically, the longest transmitting distance away from a receiving terminal for one sensing node is 2.1 km. By utilizing several nodes, a 2-km<sup>2</sup> region is covered. And the self-powered network exhibits great effectiveness and significance on fine, long-term, and wide-area environment monitoring. Furthermore, we demonstrate the sensing node's working stability over half a month. Since the nodes are portable and the embedded sensors are customizable, we anticipate that the system can be multifunctional and applied in many natural areas, such as forest, prairie, mountains, lakes regions, and so on.

### 4. Experimental Section

**The Fabrication of Wind-TEG:** The whole TENG was comprised of commercial and industrialized products. The components included a wind mill, a PCB board (FR4, 1.4 mm in thickness, 180 mm in diameter), three elongate fiber strips (polyester, 1.5 mm in height), a bearing (6200CE 2RS), acrylic plate (1 mm in thickness, 180 mm in diameter), roller (10 mm in diameter, 120 mm in length), and shell (5 mm in thickness, 200 mm in diameter). The roller was connected to the wind mill and the gear was implanted to the top of the acrylic shell. Then the roller was fixed through the gear to couple the wind mill and the TENG.

Fabrication of wind-TEG began with three elongated fiber strips stick to the gap of the PCB electrode as stator. The stator was rigid stick to the top of the acrylic shell. Subsequent CO<sub>2</sub> laser cutter was used to fabricate a FEP (100 μm in thickness) coated acrylic plate as rotor leaving 6 FEP sectors on it. Later, a gap (around 1 mm) was defined between stator and rotor by fixing the rotor on the roller, which makes slightly contact between the fiber and FEP film. Finally, the acrylic shell was sealed with hot glue to enclose the TENG structure. And some desiccant (Ringchaowei) was used to keep the fiber dry.

**The Fabrication of PMU and Transmitter:** The PCB of PMU and transmitter were fabricated by FR4 with the thickness 1.2 and 1.6 mm respectively. The detailed circuit information is summarized in Figures S6 and S10 (Supporting Information). As for the transmitter, temperature, humidity and atmospheric pressure sensor communicate with main chip by IIC protocol. The communication frequency was 433 MHz and the transmitter operated at long range mode with a baud rate 625 bps.

**The Fabrication of the Terminal Receiver:** As for the hardware, the terminal PCB was fabricated by FR4 with thickness 1.6 mm (Figure S10, Supporting Information). A sub-1G module (CC1310) and a blue tooth module (CC2540) were mounted to PCB by stamp hole. As for the software, CC1310 and CC2540 were all exploited by IAR. As for the working mechanism, the main chip CC1310 was kept searching for the different transmitter depending on MAC address. Once the data are received, it will be sent to blue tooth module through UART then retransferred to the cell phone.

The discrete components and PCB information of PMU, transmitter, and terminal receiver are summarized in Table S2 and Table S3 (Supporting Information), respectively.

**The Development of the Mini-Program:** A mini-program implant in wechat was chosen to exploit for its lightweight, simplicity, and convenient. The mini-program was developed by using Weixin Mark Language (WXML), Weixin Style Sheet (WXSS), and JavaScript (JS). And the mini-program operated on the platform of wechat 7.0.22 based on Android 9. The mechanism of the mini-program was to keep communicating with the terminal receiver through BLE and update the sensing data in real time.

**The Tests in Laboratory:** For the output performance of wind-TEG were tested through an electrometer KEITHLEY 6517. A high voltage probe (HVP-40) was connected in parallel with wind-TEG when measure the  $V_{oc}$  (Figure S2, Supporting Information). During the

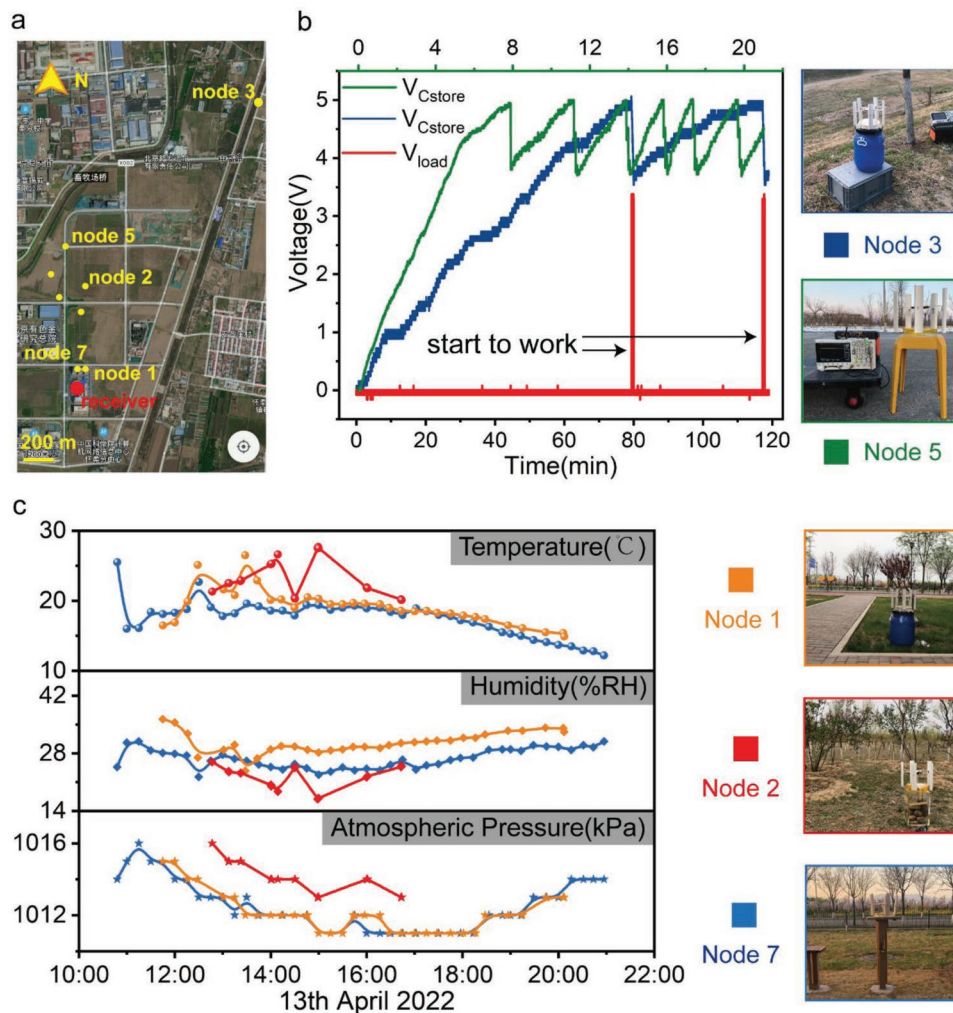


**Figure 5.** The experiences of the self-powered wireless monitoring nodes. a) Schematic distribution of the monitoring nodes. b) Voltage variation of node 3 (green curve) and node 5 (blue curve) under moderate breeze and gentle breeze respectively. The red curve illustrates the UVLO's power supply for terminal corresponding to the blue curve. c) The data acquired from nodes 1, 2, 7 lasting for 12 h.

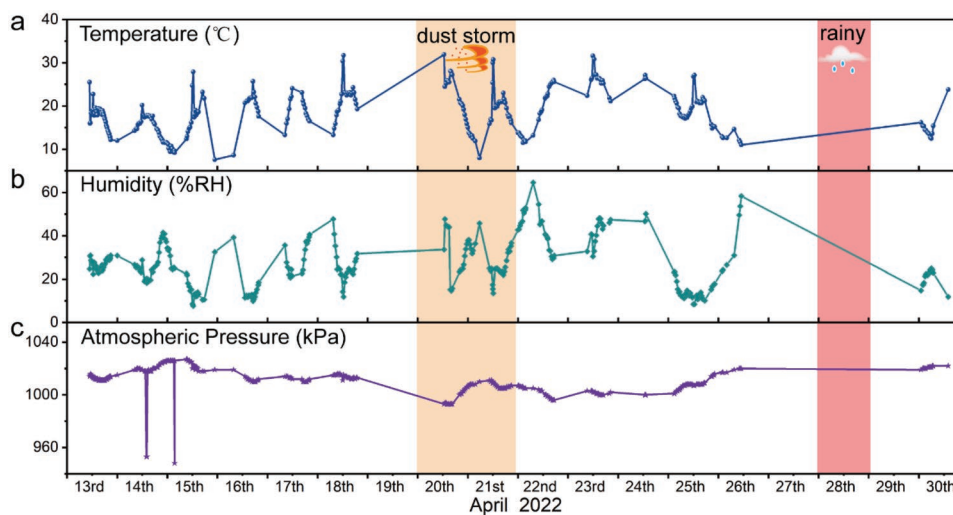


**Figure 6.** The results of long-term environment monitoring. Continuous a) temperature, b) humidity, and c) atmospheric pressure's monitoring by node 7 for more than half a month.

process of the test, different speeds of wind were supplied by a fan (POPULA SHT2.5A) to mimic the input wind energy. Except the  $V_{oc}$ ,  $Q_{sc}$  and a part of the durability measurement, the rest were tested with a constant wind speed  $3 \text{ m s}^{-1}$ . The torque was measured by DYN-200 while the TENG were actuated by a motor. The brand of commercial thermohygrometer was MIUI.

*The Tests in Natural Environment:* For the self-powered thermohygrometer measurement, the wind-TENG was placed on a balcony exposed to natural wind and an anemometer (BENETECH GM8902+) was used to record the wind speed in real time.

For the long transmission distance monitoring, a mobile battery (DXPOWER) was used to power the oscilloscope (KEYSIGHT DSO-X 2014A), which is used to sample the voltage of the capacitor and the load of the node. The sample rate was  $100 \text{ Sa s}^{-1}$  and the real-time data were saved in U-disk. The node 5 with a transmission distance 1.1 km located at a crossroad while another node 3 with a transmission distance 2.1 km located at a riverbank. Both two locations have few shelters such as trees or buildings.

*For the Distributed Wide-Area Environment Monitoring:* Node 1 with a transmission distance 100 m located beside a road. The node 7 with a transmission distance 120 m located between two buildings and the node 2 with a transmission distance around 780 m was placed to a small hill with wide open area. In order not to be destroyed by the heavy wind, node 1 was rigid fixed on a steel volume, while nodes 2 and 7 were mounted to a cylindrical container filled with rock.

*For the Long-Term Environment Monitoring:* Node 7 was placed for 18 days without maintenance and the monitoring curves were plotted by the data with a sample about half an hour.

All of the data and data graph are processed by using Origin 2018.

## Supporting Information

Supporting Information is available from the Wiley Online Library or from the author.

## Acknowledgements

D.L. and C.L. contributed equally to this work. This work was supported by the National Key R&D Project from Minister of Science and Technology (2021YFA1201601), National Natural Science Foundation of China (Grant Nos. 51432005 and 5151101243), and Youth Innovation Promotion Association, CAS.

## Conflict of Interest

The authors declare no conflict of interest.

## Data Availability Statement

The data that support the findings of this study are available from the corresponding author upon reasonable request.

## Keywords

distributed networks, environmental monitoring, self-powered, sustainability, wireless nodes

Received: August 6, 2022  
Revised: October 19, 2022  
Published online:

- [1] S. C. Elmendorf, G. H. R. Henry, R. D. Hollister, *Nat. Clim. Change* **2012**, 2, 453.
- [2] C. E. Langlais, A. Lenton, S. F. Heron, C. Evenhuis, A. Sen Gupta, J. N. Brown, M. Kuchinke, *Nat. Clim. Change* **2017**, 7, 839.
- [3] M. L. Noon, A. Goldstein, J. C. Ledezma, P. R. Roehrdanz, S. C. Cook-Patton, S. A. Spawn-Lee, T. M. Wright, M. Gonzalez-Roglich, D. G. Hole, J. Rockström, W. R. Turner, *Nat. Sustainability* **2021**, 5, 37.
- [4] T. Amano, T. Székely, H. S. Wauchope, B. Sandel, S. Nagy, T. Mundkur, T. Langendoen, D. Blanco, N. L. Michel, W. J. Sutherland, *Nat. Clim. Change* **2020**, 10, 959.
- [5] A. Depicker, L. Jacobs, N. Mboga, B. Smets, A. Van Rompaey, M. Lennert, E. Wolff, F. Kervyn, C. Michellier, O. Dewitte, G. Govers, *Nat. Sustainability* **2021**, 4, 965.
- [6] L. Shi, I. Kloog, A. Zanobetti, P. Liu, J. D. Schwartz, *Nat. Clim. Change* **2015**, 5, 988.
- [7] E. P. Fenichel, S. A. Levin, B. McCay, K. S. T. Martin, J. K. Abbott, M. L. Pinsky, *Nat. Clim. Change* **2016**, 6, 237.
- [8] D. L. McCollum, V. Krey, K. Riahi, *Nat. Clim. Change* **2011**, 1, 428.
- [9] J. P. W. Scharlemann, R. C. Brock, N. Balfour, C. Brown, N. D. Burgess, M. K. Guth, D. J. Ingram, R. Lane, J. G. C. Martin, S. Wicander, V. Kapos, *Sustainability Sci.* **2020**, 15, 1573.
- [10] A. Meque, S. Gamedze, T. Moitlhobogi, P. Booneedy, S. Samuel, L. Mpalang, *Clim. Serv.* **2021**, 23, 100243.
- [11] P. Jain, D. Castellanos-Acuna, S. C. P. Coogan, J. T. Abatzoglou, M. D. Flannigan, *Nat. Clim. Change* **2021**, 12, 63.
- [12] M. J. L. Peers, Y. N. Majchrzak, A. K. Menzies, E. K. Studd, G. Bastille-Rousseau, R. Boonstra, M. Humphries, T. S. Jung, A. J. Kenney, C. J. Krebs, D. L. Murray, S. Boutin, *Nat. Clim. Change* **2020**, 10, 1149.
- [13] S. Sippel, N. Meinshausen, E. M. Fischer, E. Székely, R. Knutti, *Nat. Clim. Change* **2020**, 10, 35.
- [14] P. Singh, *Int. J. Eng. Sci.* **2018**, 6, 629.
- [15] M. A. Akkaş, R. Sokullu, *Procedia Comput. Sci.* **2017**, 113, 603.
- [16] P. Rajendran, H. Smith, *Adv. Mater. Res.* **2015**, 1125, 641.
- [17] C. Lupangu, R. C. Bansal, *Renewable Sustainable Energy Rev.* **2017**, 73, 950.
- [18] J. D. Knapp, P. G. Flikkema, *Global Internet of Things Summit (GloTS)*, IEEE, Geneva, Switzerland, **2017**, p. 195.
- [19] K. Ameku, B. M. Nagai, J. N. Roy, *Exp. Therm. Fluid Sci.* **2008**, 32, 1723.
- [20] D. P. Kadam, B. E. Kushare, *Int. J. Eng. Sci. Adv. Technol.* **2012**, 2, 1076.
- [21] W. C. He, W. L. Liu, S. K. Fu, H. Y. Wu, C. C. Shan, Z. Wang, Y. Xi, X. Wang, H. Y. Guo, H. Liu, C. G. Hu, *Research* **2022**, 2022, 9812865.
- [22] X. K. Yu, S. K. Fu, X. L. Zuo, J. Zeng, C. C. Shan, W. C. He, W. P. Li, C. G. Hu, *Adv. Funct. Mater.* **2022**, 32, 2207498.
- [23] H. Chen, C. Xing, Y. Li, J. Wang, Y. Xu, *Sustainability Energy Fuels* **2020**, 4, 1063.
- [24] S. Lu, L. Gao, X. Chen, D. Tong, W. Lei, P. Yuan, X. Mu, H. Yu, *Nano Energy* **2020**, 75, 104813.
- [25] D. Z. Zhang, Z. M. Yang, P. Li, M. S. Pang, Q. Z. Xue, *Nano Energy* **2019**, 65, 103974.
- [26] D. Y. Wang, D. Z. Zhang, J. Y. Guo, Y. Q. Hu, Y. Yang, T. H. Sun, H. Zhang, X. H. Liu, *Nano Energy* **2021**, 89, 106410.
- [27] D. Y. Wang, D. Z. Zhang, Y. Yang, Q. Mi, J. H. Zhang, L. D. Yu, *ACS Nano* **2021**, 15, 2911.
- [28] Y. Su, G. Xie, S. Wang, H. Tai, Q. Zhang, H. Du, H. Zhang, X. Du, Y. Jiang, *Sens. Actuators, B* **2017**, 251, 144.
- [29] Y. T. Jao, P. K. Yang, C. M. Chiu, Y. J. Lin, S. W. Chen, D. Choi, Z. H. Lin, *Nano Energy* **2018**, 50, 513.
- [30] Y. Liu, W. Yan, J. Han, B. Chen, Z. L. Wang, *Adv. Funct. Mater.* **2022**, 32, 2202964.
- [31] K. Zhao, G. Gu, Y. Zhang, B. Zhang, F. Yang, L. Zhao, M. Zheng, G. Cheng, Z. Du, *Nano Energy* **2018**, 53, 898.
- [32] Y. Su, G. Xie, H. Tai, S. Li, B. Yang, S. Wang, Q. Zhang, H. Du, H. Zhang, X. Du, Y. Jiang, *Nano Energy* **2018**, 47, 316.

- [33] D. Liu, B. Chen, J. An, C. Li, G. Liu, J. Shao, W. Tang, C. Zhang, Z. L. Wang, *Nano Energy* **2020**, *73*, 104819.
- [34] F. Xi, Y. Pang, G. Liu, S. Wang, W. Li, C. Zhang, Z. L. Wang, *Nano Energy* **2019**, *61*, 1.
- [35] L. Xu, W. Xuan, J. Chen, C. Zhang, Y. Tang, X. Huang, W. Li, H. Jin, S. Dong, W. Yin, Y. Fu, J. Luo, *Nano Energy* **2021**, *83*, 105814.
- [36] J. Chen, W. Xuan, P. Zhao, U. Farooq, P. Ding, W. Yin, H. Jin, X. Wang, Y. Fu, S. Dong, J. Luo, *Nano Energy* **2018**, *51*, 1.
- [37] Y. Feng, K. Han, T. Jiang, Z. Bian, X. Liang, X. Cao, H. Li, Z. L. Wang, *Nano Res.* **2019**, *12*, 2729.
- [38] J. Han, Y. Feng, P. Chen, X. Liang, H. Pang, T. Jiang, Z. L. Wang, *Adv. Funct. Mater.* **2021**, *32*, 2108580.
- [39] K. Han, J. Luo, J. Chen, B. Chen, L. Xu, Y. Feng, W. Tang, Z. L. Wang, *Microsyst. Nanoeng.* **2021**, *7*, 7.
- [40] E. Kurt, F. Cottone, Y. Uzun, F. Orfei, M. Mattarelli, D. Özhan, *Int. J. Hydrogen Energy* **2017**, *42*, 17813.
- [41] X. Fu, S. Xu, Y. Gao, X. Zhang, G. Liu, H. Zhou, Y. Lv, C. Zhang, Z. L. Wang, *ACS Energy Lett.* **2021**, *6*, 2343.
- [42] S. Yong, J. Wang, L. Yang, H. Wang, H. Luo, R. Liao, Z. L. Wang, *Adv. Energy Mater.* **2021**, *11*, 2101194.
- [43] D. A. Howey, A. Bansal, A. S. Holmes, *Smart Mater. Struct.* **2011**, *20*, 085021.
- [44] F. Fei, W. J. A. Li, *Int. Conf. Robotics Biomimetics*, IEEE, Guilin, China, **2009**, p. 580.
- [45] S. Xu, X. Fu, G. Liu, T. Tong, T. Bu, Z. L. Wang, C. Zhang, *iScience* **2021**, *24*, 102318.
- [46] J. M. Wallace, V. H. Peter, *Atmospheric Science*, Academic Press, USA, **2006**.